26th INTERNATIONAL CONGRESS ON SOUND AND VIBRATION
7-11 July 2019, Montreal

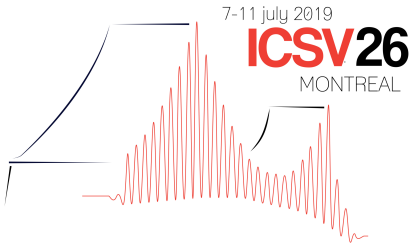

A PARAMETRIC STUDY ON WALL PRESSURE WAVENUMBER-SPECTRUM MODELS WITH APPLICATION TO AIRCRAFT FUSELAGE VIBRATION PREDICTION

Nan Hu
German Aerospace Center, Institute of Aerodynamics and Flow Technology, Braunschweig, Germany
email: nan.hu@dlr.de

Sören Callsen
Airbus Operations GmbH, Acoustic Engineer, Hamburg, Germany

email: soeren.callsen@airbus.com

The wall pressure wavenumber spectra on an aircraft fuselage are calculated analytically and numerically through two-dimensional Fourier transform of the cross-spectral models. The coherence lengths in the streamwise and spanwise directions and the convection velocity required in the cross-spectral models are provided from a flight test with DLR's research aircraft ATRA-A320. A parametric study on the coherence lengths, the convection velocity and the flow angle is performed on the analytical wavenumber-spectrum formulation. The impact of the surface microphone array size and resolution, noise and window function on the derived wavenumber spectra is studied by comparing numerical with analytical results. The fuselage vibration according to different wavenumber-spectrum formulations and the measured spectra as excitation sources is calculated with Statistical Energy Analysis. The obtained vibration spectra in one-third octave bands are compared to the measured vibration spectra. The effect of the parametric changes in the wavenumber-spectral model on the resulting wavenumber spectra is illustrated. Furthermore, the impact of the wavenumber spectra change on the resulting vibration spectra is studied and discussed.

1. Introduction

Turbulent boundary layer induced wall pressure fluctuations exert an unsteady loading on the aircraft fuselage and consequently the induced fuselage panel vibration radiates noise into the cabin, which makes the wall pressure fluctuations a major noise source for the aircraft cabin [1]. Besides the one-point excitation power, the two-point statistics of the wall pressure fluctuations are important for the excitation. Features relevant to the excitation are the coherence lengths and the convection velocity. Cross-spectral models such as the Corcos model [2] and the Smol'yakov model [3] have been developed based on applying these parameters. Based on the cross spectrum, the wavenumber spectrum can be calculated. Taking the wavenumber spectrum as the excitation source, the Statistical Energy Analysis (SEA) method can be used to calculate the surface vibration. Due to SEA's efficiency, applications in a large calculation area and for high frequencies can be performed with low cost.

A precise prediction of the coherence lengths and the convection velocity is the key for a good prediction of the coherence. However, the measurement results [4, 5] showed that the prediction accuracy of these parameters is not satisfactory. In practice, the applied surface microphone array size, resolution or the signal to noise ratio can produce additional error in calculation of the wavenumber spectrum in the post processing.

In this work, parametric modifications are performed on the wavenumber spectral formulation of the Smol'yakov model. The corresponding impact of the wavenumber spectral change on the surface vibration is illustrated by means of the SEA calculation. Furthermore, error due to the post processing involved in the wavenumber spectrum and the surface vibration is studied.

2. Theoretical approach

2.1 Cross-spectral model

Based on the coherence lengths and the convection velocity of the wall pressure fluctuations, the coherence field is formulated by the Corcos model [2] as

$$\Gamma_{pp,\,Corcos}(r_1, r_3, \omega) = \exp(-|r_1|/l_1)\exp(-|r_3|/l_3)\exp(i\omega r_1/u_c), \tag{1}$$

where $r_{1,3}$ are the separation in the streamwise and spanwise directions, $l_{1,3}$ are the coherence lengths in both directions, u_c is the convection velocity and ω is the angular frequency. The formulation for the Smol'yakov model [3] reads

$$\Gamma_{pp,\,Smol'yakov}(r_1, r_3, \omega) = \exp\left(-\sqrt{(r_1/l_1)^2 + (r_3/l_3)^2}\right)\exp(i\omega r_1/u_c). \tag{2}$$

Both models use the exponential function to formulate the coherence in the streamwise and spanwise directions. The difference between the two models is the formulation on the off-axis coherence. Thus, a rhombic shaped coherence field is formulated by the Corcos model and an elliptic shaped field by the Smol'yakov model.

Taking the spatial Fourier transform of the coherence provided by Eqs. (1–2)

$$\Gamma_{pp}(k_1, k_3, \omega) = \frac{1}{(2\pi)^2}\int_{\infty}^{\infty}\int_{\infty}^{\infty}\Gamma_{pp}(r_1, r_3, \omega)\exp(ik_1 r_1)\exp(ik_3 r_3)\,\mathrm{d}r_1\mathrm{d}r_3, \tag{3}$$

where $k_{1,3}$ denote the wavenumber in the streamwise and spanwise directions. We obtain the wavenumber spectra for the Corcos model and the Smol'yakov model,

$$\Gamma_{pp,\,Corcos}(k_1, k_3, \omega) = \frac{l_1 l_3}{\pi^2}\frac{1}{(1 + l_1^2(k_1 - \omega/u_c)^2)(1 + l_3^2 k_3^2)}, \tag{4}$$

$$\Gamma_{pp,\,Smol'yakov}(k_1, k_3, \omega) = \frac{l_1 l_3}{2\pi}\frac{1}{(1 + l_1^2(k_1 - \omega/u_c)^2 + l_3^2 k_3^2)^{3/2}}. \tag{5}$$

If the flow direction is not aligned with the applied array coordinate system, an inclination of the wavenumber spectrum would be present. Furthermore, due to the presence of different flow angles in different layers across the boundary layer, an misalignment of the convection ridge center in the wavenumber spectrum could occur, which was reported from flight tests for the fuselage region in the vicinity of the wing [6]. For those cases, the separation for the flow streamwise direction $\tilde{r}_1$ should be defined as $\tilde{r}_1 = \cos\alpha \cdot r_1 + \sin\alpha \cdot r_3$ and for the flow spanwise direction $\tilde{r}_3$ as $\tilde{r}_3 = -\sin\alpha \cdot r_1 + \cos\alpha \cdot r_3$. If the

flow convection angle is not the same as the inclination of the coherence pattern, a different angle β will be applied for the convection term. As an example, Eq. (2) is reformulated for the case with presence of flow angle as

$$\Gamma_{pp,\,Smol'yakov}(r_1, r_3, \alpha, \beta, \omega) = \exp\left(-\sqrt{(\tilde{r}_1(\alpha)/l_1)^2 + (\tilde{r}_3(\alpha)/l_3)^2}\right) \exp(i\omega\tilde{r}_1(\beta)/u_c). \tag{6}$$

Thus, the wavenumber spectrum can be obtained by taking the Fourier transform as specified in Eq. (3),

$$\begin{aligned}\Gamma_{pp,\,Smol'yakov}(k_1, k_3, \alpha, \beta, \omega) \quad = \quad & \frac{l_1 l_3}{2\pi} \frac{1}{(1 + l_1^2(k_1\cos\alpha + k_3\sin\alpha - \omega/u_c\cos(\alpha-\beta))^2 + \cdots} \\ & \frac{1}{\cdots l_3^2(k_3\cos\alpha - k_1\sin\alpha + \omega/u_c\sin(\alpha-\beta))^2)^{3/2}}\,.\end{aligned} \tag{7}$$

2.2 Statistical Energy Analysis method

The panel vibration power $\Phi_{vib.}(\omega)$ induced by the wall pressure fluctuations can be calculated with the SEA method based on a superposition of the wavenumber spectrum and the panel acceptance,

$$\Phi_{vib.}(\omega) = \frac{1}{\omega}\sum_{m,n}\frac{\Re(d_{mn})}{|d_{mn}|^2}\frac{1}{(2\pi)^2}\int_{\infty}^{\infty}\int_{\infty}^{\infty}\Phi_{pp}(\omega)\Gamma_{pp}(k_1, k_3, \omega)|S_{mn}(k_1, k_3)|^2\,\mathrm{d}k_1\mathrm{d}k_3, \tag{8}$$

where $\Phi_{pp}(\omega)$ is the power-spectrum of the wall pressure fluctuations, d_{mn} is the dimensionless panel impedance. $S_{mn}(k_1, k_3)$ is the panel acceptance and m, n denote the panel vibration modes. For a more detailed description of the SEA implementation the reader is referred to the work of Klabes [7].

3. Results

3.1 Analytical approach

In the present work, the panel vibration is calculated according to Eq. (8). The in-flight measured wall pressure power spectrum $\Phi_{pp}(\omega)$ on passenger windows (dummy windows) in the front region of the aircraft [4, 7] is applied. The panel acceptance $S_{mn}(k_1, k_3)$ and the dimensionless panel impedance d_{mn} are determined for the closest fuselage panel above the windows. The reason for not choosing the panel directly at the window area is because the complexity of the panel structure, which may introduce more uncertainty for the applied SEA method. Due to the small circumferential spacing between the window area and the chosen area, no large difference in wall pressure power and cross spectra between the two areas is expected.

Fig. 1(a) shows the measured wavenumber spectrum and Figs. 1(b–c) show the modeled spectra based on Eqs. (4-5). The measured convection ridge is well represented by both models in terms of shape, level and position. The coherence lengths and the convection velocity needed in the models are derived from the measured results. However, it is hard to assess whether the spectral shape of Fig. 1(a) is rhombic following the Corcos model or elliptic following the Smol'yakov model.

To study the effect of the parametric changes on the resulting panel vibration, the coherence lengths, the convection velocity and the flow angle are modified. The Smol'yakov model, Eq. (5), is taken as reference due to the slightly smaller deviation from the measured vibration than the Corcos model, see Fig. 2(a). The modification range of the parameters is selected based on a priori knowledge of the range of the respective parameters. Some modified spectra are shown in Figs. 1(d–h). For example, a modification $0.5l_1$ denotes that $0.5l_1$ is applied in Eq. (5) instead of l_1. A smaller coherence length results in a broader

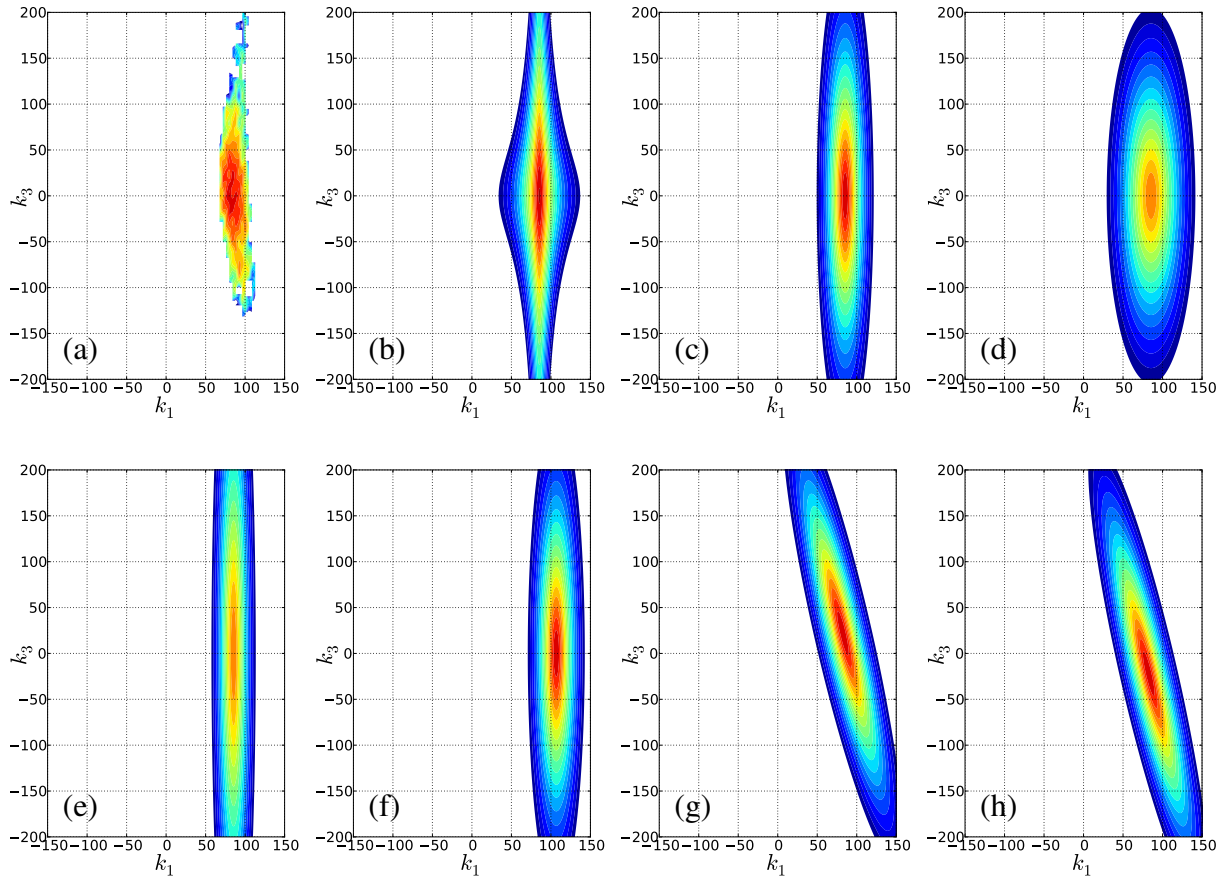

Figure 1: Wavenumber spectra $\Gamma_{pp}(k_1, k_3, \omega)$ at 2500 Hz with levels between -54 dB and -35 dB; (a) measured wavenumber spectrum; (b) Corcos model; (c) Smol'yakov model; (d–g) modifications: (d) $0.5l_1$; (e) $0.5l_3$; (f) $0.8u_c$; (g) $\alpha = 15°$, $\beta = 15°$; (h) $\alpha = 15°$, $\beta = -15°$.

spectral shape in the respective direction. A smaller convection velocity shifts the convection ridge to a higher k_1 range. For the cases with spectral inclination, Eq. (7) is applied.

Fig. 2(a) shows the difference between the measured panel vibration power and the calculated results, $10\log(\Phi^{cal.}_{vib.}(\omega)/\Phi^{meas.}_{vib}(\omega))$. The excitation sources used in the calculation are the measured wavenumber spectra $\Gamma_{pp}(k_1, k_3, \omega)$ and the formulated spectra of the two models. The averaged vibration amplitude between three accelerometers placed in different positions on the applied panel is used as reference. The gray area denotes the scatter of the measured results between the accelerometers. The calculated vibration shows large deviation at low frequencies for either the measured or the formulated spectra as the excitation source. However, the results from the formulated spectra are closer to the measured results. The reason for that is not clear to the authors. It is worth mentioning that a truncated area in k_x and k_y directions for the measured wavenumber spectra are used due to large noise at the wavenumber border area and spectral side lobes at some frequencies. This could be an issue that reduces the accuracy of the calculated vibration level.

Figs. 2(b–d) show the vibration level changes, $10\log(\Phi_{vib.}(\omega)/\Phi^{ref.}_{vib}(\omega))$, due to the parametric changes exemplified in Figs. 1(d–k). The calculated vibration result for the case with the Smol'yakov model shown in Fig. 2(a) is used as reference. The spectral change shows strong frequency dependence for all modification cases. The change between 800 Hz and 2 kHz show different trends than the rest frequencies. Outside of this range, a smaller l_1 and a larger l_3 results in a larger panel vibration level, similarly as a larger convection velocity and a large flow angle. In contrast, a larger l_1, a smaller l_3 and a smaller convection velocity lead to a smaller vibration level. This contrastive result is caused by the change of

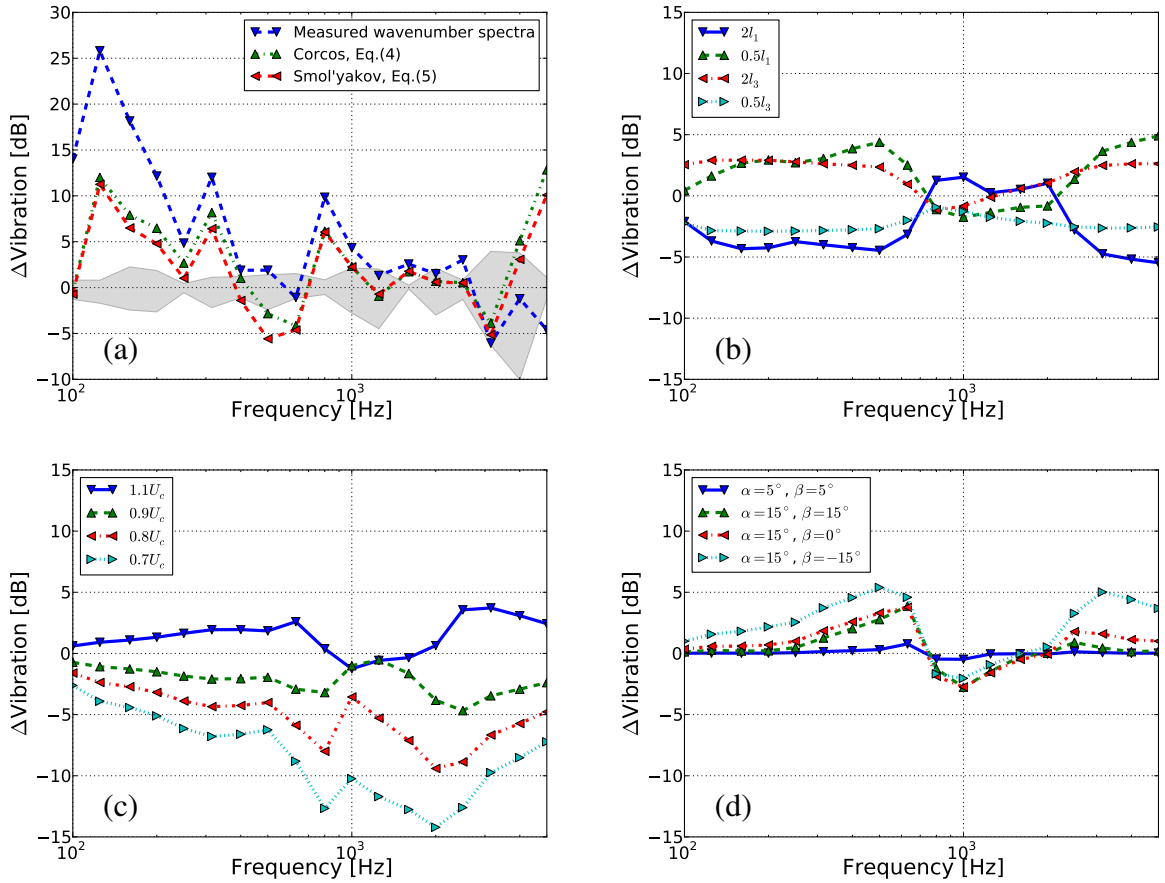

Figure 2: Comparison of panel vibration; (a) measured vs. formulated wavenumer spectra; (b–d) modifications: (b) coherence lengths; (c) convection velocities; (d) flow angles.

the wavenumber spectral feature. For example, a smaller velocity shifts the spectral convection ridge to a higher k_1 and that consequently reduces the spectral level at lower k_1 and increases the level at higher k_1, see Figs. 1(c,f). This indicates that the decrease in vibration level shown in Fig. 2(c) for a smaller convection velocity is due to the reduced spectral level at lower k_1. Note that, the change trend between 800 Hz and 2 kHz from the $1.1u_c$ case to the $0.9u_c$ case is different from the other frequencies, especially for 1 kHz and 1.25 kHz. This implies that a possible coincidence between the wall pressure convection velocity and the panel wave propagation velocity occurs within this frequency range. For the convection velocity smaller than $0.9u_c$ the vibration level reduces also in this frequency range and even with a larger level reduction. This is possibly because the panel wave propagation velocity in this frequency range is close to $0.9u_c$ and is more sensitive to a further convection velocity decrease. In contrast, at very low frequencies due to the large difference between the convection velocity and the panel wave propagation velocity, the change in vibration level is much smaller. A more detailed description of this phenomenon based on cabin noise level change in flight test can be found in Hu $et.\ al.$[1].

For the coherence length change, a smaller l_1 reduces the spectral peak level but increases spectral level at lower k_1, see Figs. 1(c–d). The larger spectral level at lower k_1 causes the increase of the vibration level outside of 800 Hz – 2 kHz. The decrease between 800 Hz and 2 kHz is probably due to the reduced peak level, and this indicates that a coincidence occurs in this frequency range.

3.2 Processing artifacts

In practice, the wavenumber spectrum is calculated through Fourier transformation of spatial coherence measured or simulated in a surface microphone array. Therefore, the post processing procedure

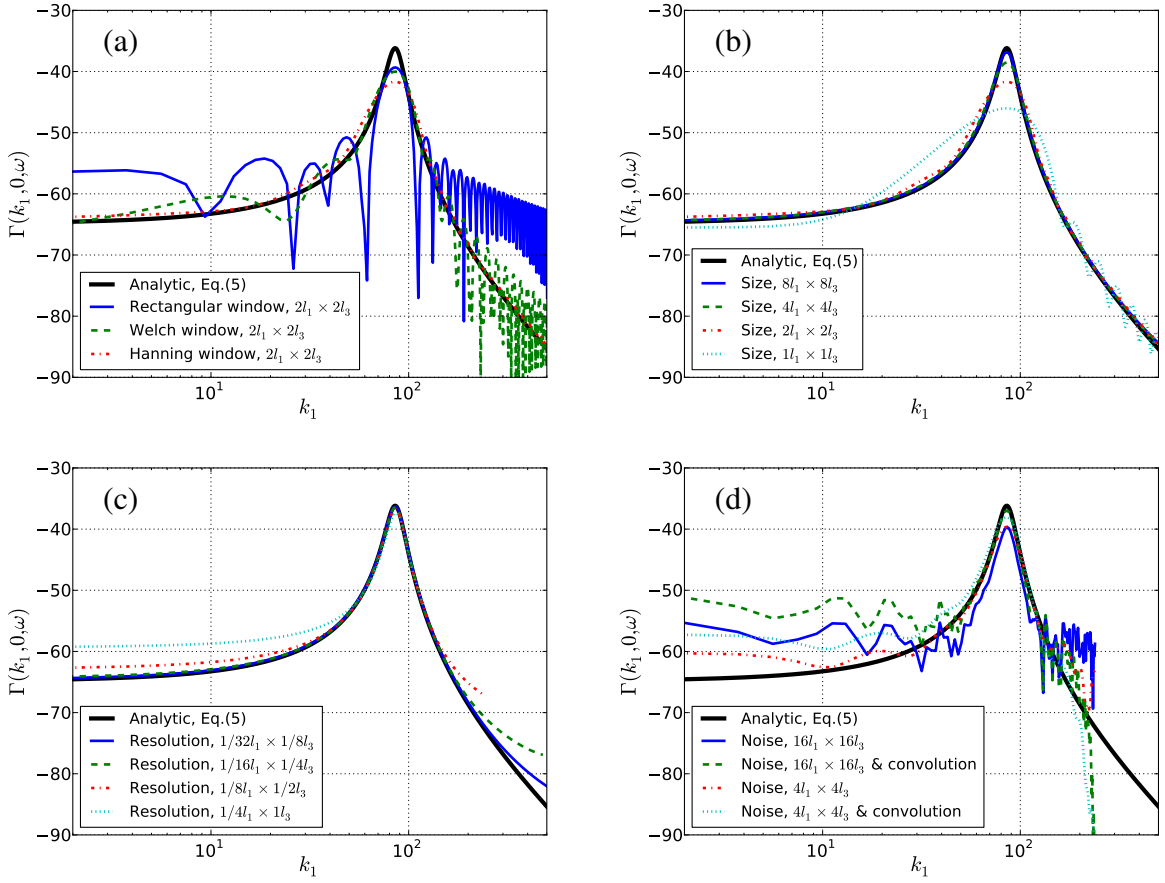

Figure 3: Comparison of wavenumber spectra $\Gamma_{pp}(k_1, 0, \omega)$ at 2500 Hz with different processing settings; (a) window functions; (b) array sizes; (c) array resolutions; (d) noisy signal.

could impact the calculation results. Here, the impact of applied window functions, array sizes, resolutions and present noise on the calculated wavenumber spectra and the resulting vibration is studied using a cartesian mesh array, which is commonly applied in simulation.

The coherence $\Gamma(r_1, r_3, \omega)$ is generated based on Eq. (2) and the wavenumber spectrum $\Gamma(k_1, k_3, \omega)$ is calculated using Fourier transformation, Eq. (3). Frequency-dependent array sizes/integration areas and resolutions are applied. In general, a large array size and a fine resolution relating to the coherence lengths are desired. However, in practice this cannot be easily realized due to the small or large coherence lengths at high or low frequencies. A large integration area is needed to obtain a fine resolution in the calculated wavenumber spectrum, which can be easily achieved by adding zero-padding outside of the array area. A window function is needed to avoid an abrupt coherence drop to zero if the array size is not large enough, e.g. for an array with a size of $2l_1 \times 2l_3$, the coherence at the array border is 0.135. Furthermore, in reality the signal is always affected by noise, which increases the error in the calculated wavenumber spectra and panel vibration. Thus, following four test cases are performed. 1, test for window functions: different window functions are applied on an array with a size of $2l_1 \times 2l_3$ and a resolution of $1/64l_1 \times 1/16l_3$. 2, test for array size: the array size is varied from $8l_1 \times 8l_3$ down to $1l_1 \times 1l_3$; the array resolution is $1/64l_1 \times 1/16l_3$. 3, test for array resolution: the array resolution is varied from $1/32l_1 \times 1/8l_3$ down to $1/4l_1 \times 1l_3$; the array size is $16l_1 \times 16l_3$. 4, test for noise: complex random noise with an amplitude of 0.05 is added in the coherence field on an array with a resolution of $1/8l_1 \times 1/2l_3$. In all test cases, the integration area is set to be $16l_1 \times 16l_3$.

Fig. 3(a) shows the calculated k_1 spectra for three applied window functions at the array size of $2l_1 \times 2l_3$. Very strong side lobes are present for the case with the rectangular window. For the case with

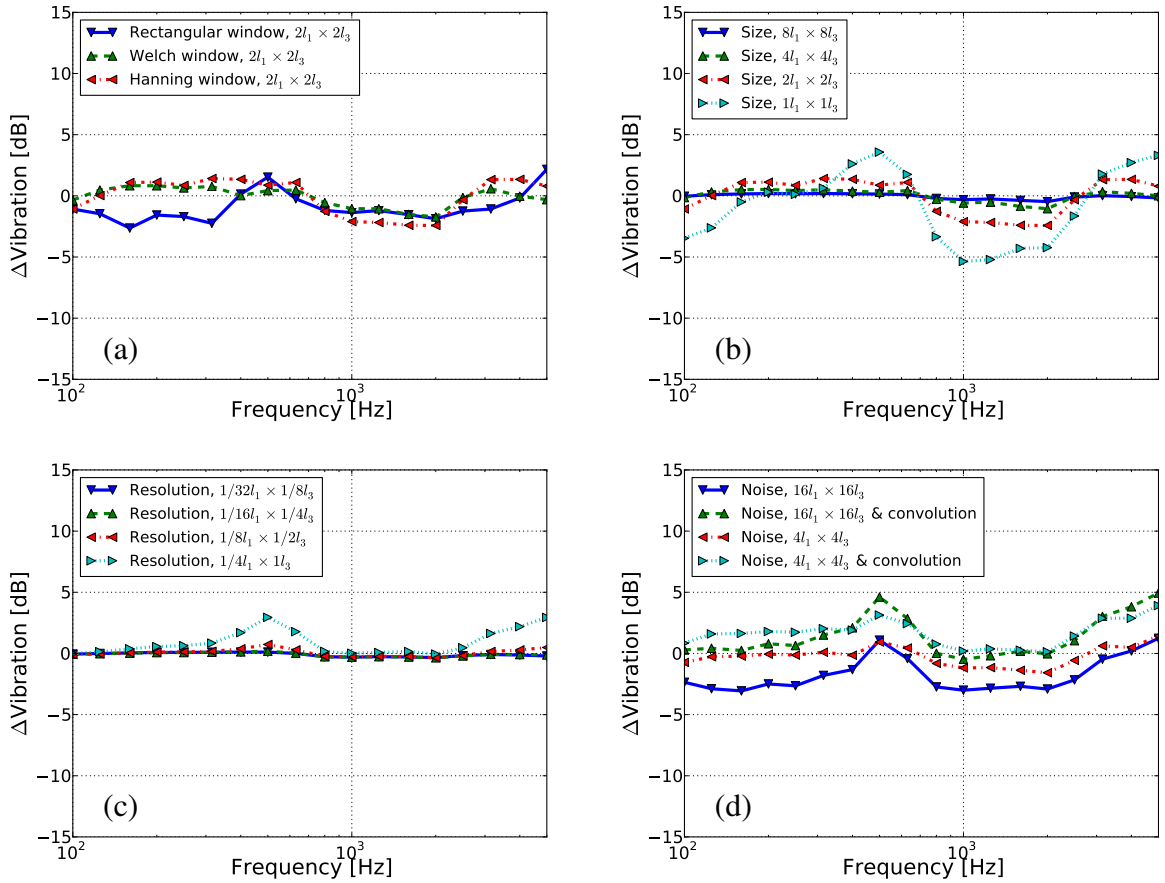

Figure 4: Comparison of panel vibration with different processing settings; (a) window functions; (b) array sizes; (c) array resolutions; (d) noisy signal.

the Hanning window a smooth spectrum is obtained, however, with an additional loss in peak level. The spectral feature for the case with the Welch window is between that of the rectangular and Hanning windows. Due to the smooth spectral behavior and an acceptable worsening of the peak level, the Hanning window is selected for the further calculations. The array size impacts the peak level and for the worst case with $1l_1 \times 1l_3$ the spectral peak is also broadened, see Fig. 3(b). Fig. 3(c) shows the impact of the array resolution. A rougher resolution increases the spectral level at lower and higher k_1. Note that, if the resolution $\mathrm{d}r_1$ is greater than $1/4l_1$, the peak may not be captured. Fig. 3(d) shows the results for the noisy signal in two different array sizes. The large array size in post processing may be used at high frequencies in practice. Furthermore, a convolution with a Gaussian blur 3×3 kernel is applied. The noise in the calculated spectra can be found at lower and higher k_1. Because all spectra are normalized, thus, a smaller peak level is caused by the present noise. With the smaller array size $4l_1 \times 4l_3$, the noise is reduced because the area outside of $4l_1 \times 4l_3$ the signal to noise ratio is very low. A further noise reduction is achieved with the convolution at higher k_1, however, with an increased spectral level at lower k_1.

Fig. 4 shows the calculated vibration compared to the reference case with the analytical excitation source provided from Eq. (5). Fig. 4(a) shows the largest deviation present for the case with the rectangular window due to its side lobes. The deviations of the Welch and Hanning windows are similar in shape, but the deviation as a result of the Welch window is generally smaller for the test case. This is probably due to the better agreement at the spectral peak region.

For the test cases without noise, a noticeable deviation is found when the array size not greater than $2l_1 \times 2l_3$ and the array resolution is $1/4l_1 \times 1l_3$. The induced vibration level decrease between 800 Hz and 2 kHz is attributed to the decrease in the spectral peak level. The level increase around 500 Hz and

for frequencies larger than 3 kHz is probably due to the increased spectral level at lower k_1. For the noisy signal case, the smaller array size provides better results. An additional convolution procedure on the smaller array increases the error outside of 800 Hz and 2 kHz, which is due to an increase of the spectral noise level at lower k_1. Note that, dealing with noisy signal the side lobes produced by the Welch window may have a larger impact on the resulting vibration level. Therefore, the produced error may be larger than that by the Hanning window.

4. Conclusion

The wall pressure wavenumber spectra in the front region of the aircraft fuselage in cruise condition are formulated with the wall pressure cross-spectral model. The formulated spectra are used as excitation sources for calculation of the fuselage panel vibration with the Statistical Energy Analysis method. The coherence length, the convection velocity and the flow angle are modified to study their effects on the resulting wavenumber spectrum and the panel vibration. Furthermore, the impact of some important factors on the calculated results in practice such as the microphone array size and resolution, window functions and dealing with noisy signal is studied.

The results show that a modification of the wall pressure parametric changes the wavenumber spectral shape or position, which impacts the panel vibration level. For the frequencies between 800 Hz and 2 kHz in which a possible coincidence between the flow excitation and the panel vibration occurs, the wavenumber spectral peak region is important for the excitation. A change in the spectral peak level results in a respective change in panel vibration level. For frequencies outside of 800 Hz – 2 kHz, it is found that the lower streamwise wavenumber spectral range is important for the fuselage panel excitation.

In practice, an array with a resolution finer than 1/4 the streamwise coherence length and one spanwise coherence length and an array with a size larger than twice the coherence lengths in respective directions are recommend. Dealing with noisy signal, an overly large array size will increase the error of the calculated wavenumber spectra and panel vibration due to an increase of the data processing area with a low signal to noise ratio.

REFERENCES

1. Hu, N., Buchholz, H., Herr, M., Spehr, C. and Haxter, S. Contributions of different aeroacoustic sources to aircraft cabin noise, *AIAA Paper 2013-2030*, (2013).

2. Corcos, G. M. The Structure of the Turbulent Pressure Field in Boundary Layer Flows, *J. Fluid Mech.*, **18**, 353–378, (1964).

3. Smol'yakov, A. V. and Tkachenko, V. M. Model of a field of pseudosound turbulent wall pressures and experimental data, *Akust. Zh*, **37**, 1199–1207, (1991).

4. Haxter, S. and Spehr, C. Comparison of model predictions for coherence length to in-flight measurements at cruise condition, *J. Sound Vib.*, **390**, 86–117, (2017).

5. Haxter, S., Brouwer, J., Sesterhenn, J. and Spehr, C. , Obtaining phase velocity of turbulent boundary layer pressure fluctuations at high subsonic Mach number from wind tunnel data affected by strong background noise, *J. Sound Vib.*, **402**, 85–103, (2017).

6. Haxter, S., Berkefeld, T. and Spehr, C. Determining flow propagation direction from in-flight array surface pressure fluctuation data, *AIAA Paper 2017-3205*, (2017).

7. Klabes, A., Aircraft fuselage vibration excitation by turbulent boundary layer flow in cruise, *PhD thesis*, Institute of Aerodynamics and Flow Technology, Germany Aerospace Center, (2017).